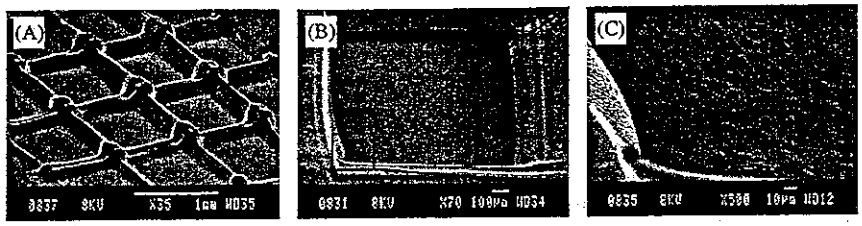

Fig. 8. SEM images of cell-seeded multi-microwells prepared from P(T/P200) on a glass surface: (A) multi-microwells and (B) and (C) microphotograph of a cell adhering only to the glass surface.

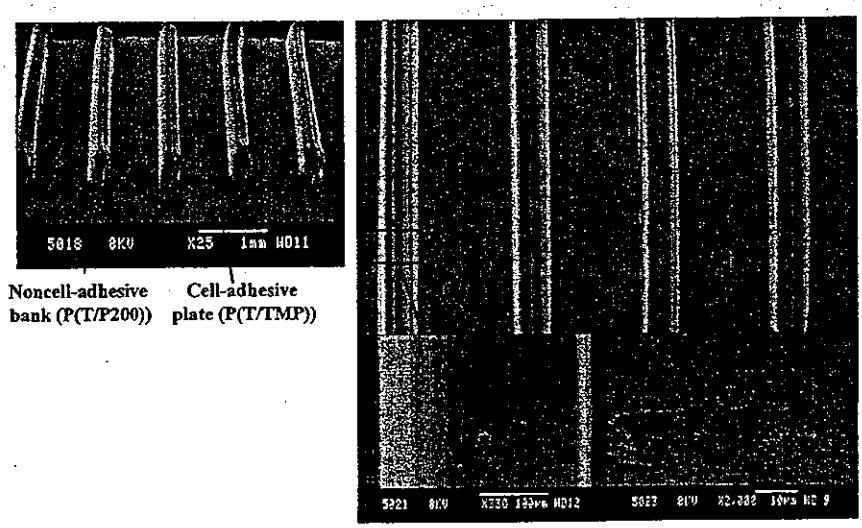

Fig. 9. SEM images of composite construct composed of a plate with cell-adhesive P(T/TMP) and microbanks with noncell-adhesive P(T/P200).

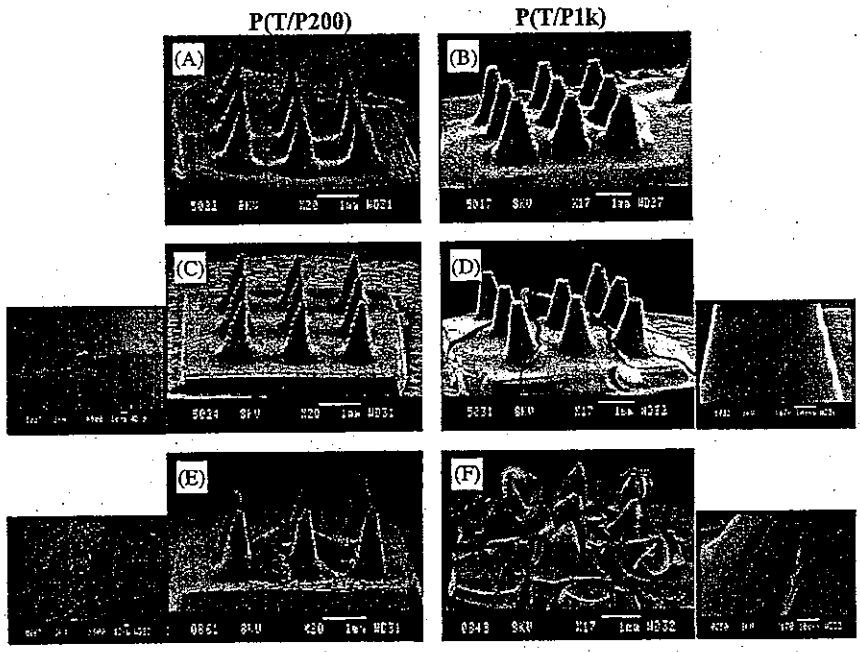

Fig. 10. SEM images of microcone array composed of P(T/P200) or P(T/P1k) implanted under the dorsal subcutis of a rat. Before implantation (A, B), at 1-week implantation (C, D) and at 4-week implantation (E, F).

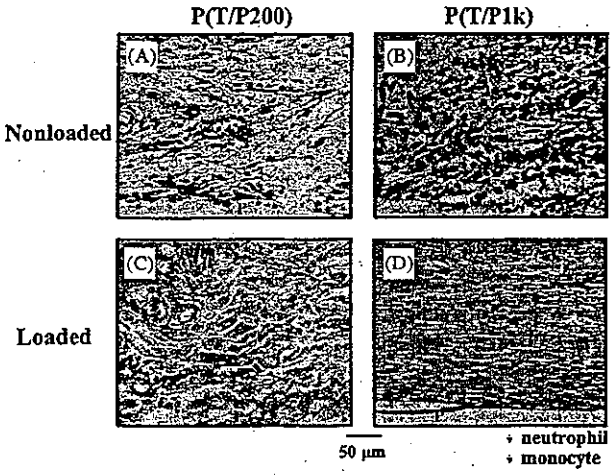

Fig. 11. Histological cross-sectional microphotographs of subcutaneous tissues surrounding the implanted photo-polymerized construct at 1-week implantation; nonloaded (A, B) and dexamethasone-loaded (C, D).

highly swellable P(T/P1k) and poorly swellable P(T/P200). The nonloaded or drug-loaded microcone arrays were implanted under the dorsal subcutis of rats and the surrounding tissues of implanted photo-polymerized constructs at 1-week implantation were harvested. Differences in the features of tissues surrounding the constructs between nonloaded and dexamethasone-loaded microcone arrays and also between P(T/P1k)- and P(T/P200)-derived microcone arrays were observed. A large number of fibroblasts and leucocytes, such as neutrophils and monocytes, induced due to the foreign-body antigenic inflammatory reaction invaded into the subcutis surrounding the nonleaded construct made of P(T/P1k) (Fig. 11B). The extent of foreign-body inflammatory reaction decreased in the order: nonloaded P(T/P1k)-based $\gg$ nonleaded P(T/P200)-based > drug-loaded P(T/P200)-based $\gg$ drug-loaded P(T/P1k)-based. Irrespective of the type of construct, drug-loading significantly reduced the invasion of cells into the surrounding tissues (Fig. 11). Such a tendency was more prominent for P(T/P1k) than for P(T/P200). Leucocytes were hardly observed in tissues surrounding the drug-loaded construct made of P(T/P1k) (Fig. 11D). This indicates that photo-polymerized construct made of drug-loaded P(T/P1k) minimized the inflammatory reaction.

4. Discussion

SL using the layer-by-layer photo-fabrication method, which employs computer-aided manufacturing (CAM), light beam, and photo-polymerizable prepolymers, allows the generation of complex 3D constructs [1-4]. Using the SL technique, various medical applications, such as photo-polymerized constructs of micro-architectural surfaces and precision micro- and macroshaped devices for drug delivery matrices, implants and scaffolds for engineered tissues may be feasible using biocompatible biodegradable photo-polymerizable liquid prepolymers with the ability to rapidly solidify upon UV irradiation, but only few applications have been utilized [10,17]. For biomedical applications, the design of photo-polymerizable biocompatible liquid prepolymers is essentially required. However, only a few studies on such prepolymers were reported. Along with the design criteria satisfying the requirements for biomedical applications, we prepared multi-functional liquid prepolymers based on TMC and CL, which were capped with an acrylate group at the ends, because both TMC and CL can be metabolized in the body. Cooke et al. has developed a 3D photo-polymerized bone substrate, the external surface and internal geometry of which was of the actual size for implantation (50 mm diameter and 4 mm thick), prepared from a biodegradable poly(propylene fumarate) (PPF) with a photo-initiator using a commercially available SLA device [17].

In our previous study, we synthesized biodegradable liquid acrylated TMC-based prepolymers, which were initiated by tri-ol (TMP) or linear PEGs with a mol. wt. of 200 or 1000, and then evaluated the photo-polymerizing characteristics and hydrolytic behavior after photo-polymerization by visible-light irradiation; the photo-polymerized films derived from a low molecular weight PEG (PEG200) and TMP exhibited a much lower hydrolysis potential than PEG1000-derived polymers in terms of weight loss, water uptake, swelling depth, and micromechanical properties of the surface [18].

In this article, precisely designed microarchitectures were photo-polymerized using the three different acrylated liquid prepolymers [T/P200, T/P1k, and T/TMP], which exhibited liquid-to-solid transformation within 10–20 s of UV-irradiation at a photo-intensity of 2 W/cm^2 at 365 nm, irrespective of prepolymer (Table 1 and Fig. 3). Our custom-designed μSL apparatus consisted of a movable light pen for the x and y axes with a photo-mask, a movable table for the z axis, UV-light source, and liquid prepolymer bath operated using the CAD/CAM system was useful for photo-polymerizing microscale constructs as evidenced in the SEM images, such as the micropillar array, microcone array, microbank array, and multi-microtunnels, which may have possible applications such as the microarchitectural surfaces for drug releasing or the cell platform for guidance and the 3D spatio-regiospecific segregation matrix for tissue engineering (Figs. 5 and 6).

Our results showed that PEG-based hydrophilic photo-polymerized films [P(T/P200) and P(T/P1k)],

whose receding contact angles were 27° and less than 5°, respectively, exhibited a very low cell adhesion potential, whereas P(T/TMP) (receding contact angle, 47.4°) exhibited high cell adhesion and proliferation potentials (Table 1 and Fig. 7). Exploiting these differences in properties between hydrophilic and relatively hydrophobic TMC-based prepolymers, functionally designed microarchitectural constructs such as multi-microwells with noncell adhesion potential (P(T/P200)) on the glass surface and composite microbank array which consisted of a cell-adhesive plate (P(T/TMP)) and noncell-adhesive banks (P(T/P200)) were photo-polymerized. Cells only adhered and spread inside the square wells (on the glass surface) in the multi-microwells (Figs. 8B and C). Well-adhered and spread cells were observed on the plate for composite microbank array, whereas cells were hardly observed on the PEG-based prepolymer-derived banks (Fig. 9). Regarding drug-releasing micro-architectured surfaces, implanted microcone arrays impregnated with or without an anti-inflammatory drug, dexamethasone, affected the polymer-dependent degree of foreign-body inflammatory reactions, which induced neutrophils, monocytes, lymphocytes, and fibroblasts. The degree of reaction was decreased in the order: nonloaded P(T/P1k)-based $\gg$ nonloaded P(T/P200)-based > drug-loaded P(T/P200)-based $\gg$ drug-loaded P(T/P1k)-based (Fig. 11). This tendency is probably due to the different hydrolytic characteristics of the two polymers such as degree of water adsorptivity (2% for P(T/P200) and 30% for P(T/P1k), respectively) and degradation rate in vivo (Table 1 and Fig. 10). That is, a highly swellable and fast degradable P(T/P1k)-based photo-polymerized construct can take up and release a large amount of an aqueous drug solution than a poorly swellable and slow degradable P(T/P200)-based construct.

5. Conclusion

In this study, precisely and functionally designed microarchitectural constructs made of photo-polymerizable biodegradable TMC-based liquid prepolymers have been photo-polymerized using a custom-designed μSL apparatus automated by CAD system. The μSL-driven photo-polymerized construct having a wide scope of hydrolytic characteristics and cell adhesive/noncell adhesive properties can provide advanced precision microfabricated devices for drug delivery matrices, implants and engineered tissues. Our next target using μSL with these liquid prepolymers is to fabricate a few tenths micron-order microneedle-array-covered stent to minimize excessive tissue ingrowth (intimal hyperplasia) in atherosclerotic vessels, which will be realized using a μSL two-photon system.

Acknowledgements

The authors thank Dr. S. Imayama (MD), Department of Dermatology, Kyushu National Hospital, for the histological analysis and Dr. T. Kanemaru of the Faculty of Medicine, Kyushu University, for SEM. This study was financially supported in part by a Grant-in-Aid for Scientific Research (A2-15200038) from MEXT, Japan.

References

[1] Kodama H. Automatic method for fabricating a three-dimensional plastic model with photohardening polymer. Rev Sci Instrum 1981;52:770–3.
[2] Herbert AJ. Solid object generation. J Appl. Photographic Eng 1982;8:185–8.
[3] Yakunin VP. Laser stereolithography as a wasteless technology for rapid layer by layer production of parts from liquid polymers. Liteinoe Proizvodstvo 1999;7:5–6.
[4] Kulkarni RB, Manners CR. Stereolithographic process of making a threedimensional object. US Patent No. 6,558,606, 2003.
[5] Eufinger H, Wehmoller M, Machtens E, Heuser L, Harders A, Kruse D. Reconstruction of craniofacial bone defects with individual alloplastic implants based on CAD/CAM-manipulated CT data. J Craniomaxillofac Surg 1995;23:175–81.
[6] Eufinger H, Pack M, Terheyden H, Wehmoller M. Experimental computer-assisted alloplastic sandwich augmentation of the atrophic mandible. J Oral Maxillofac Surg 1999;57:1436–41.
[7] Poulsen M, Lindsay C, Sullivan T, D'Urso P. Stereolithographic modeling as an aid to orbital brachytherapy. Int J Radiat Oncol Biol Phys 1999;44:731–5.
[8] Binder TM, Moertl D, Mundigler G, Rehak G, Franke M, Delle-Karth G, Mohl W, Baumgartner H, Maurer G. Stereolithographic biomodeling to create tangible hard copies of cardiac structures from echocardiographic data: *in vitro* and *in vivo* validation. J Am Coll Cardiol 2000;35:230–7.
[9] Hutmacher D. Scaffold design and fabrication techniques for engineering tissues-state of the art future perspectives. J Biomater Sci Polym Edn 2001;12:107–24.
[10] Cooke MN, Fisher JP, Dean D, Rimnac C, Mikos AG. Use of stereolithography to manufacture critical-sized 3D biodegradable scaffolds for bone ingrowth. J Biomed Mater Res 2002;64B:65–9.
[11] Matsuda T, Mizutani M, Arnold SC. Molecular design of photocurable liquid biodegradable copolymers. 1. Synthesis and photocuring characteristics. Macromolecules 2000;33:795–800.
[12] Matsuda T, Mizutani M. Molecular design of photocurable liquid biodegradable copolymers. 2. Synthesis of coumarin-derivatized oligo(methacrylate)s and photocuring. Macromolecules 2000;33:791–4.
[13] Mizutani M, Matsuda T. Photocurable liquid biodegradable copolymers: *in vitro* hydrolytic degradation behaviors of photocured films of coumarin-end-capped poly(ε-caprolactone-co-trimethylene carbonate). Biomacromolecules 2002;3:249–55.
[14] Mizutani M, Matsuda T. Liquid photocurable biodegradable copolymers: *in vivo* degradation of photocured poly(ε-caprolactone-co-trimethylene carbonate). J Biomed Mater Res 2002;61:53–60.
[15] Mizutani M, Arnold SC, Matsuda T. Liquid phenylazide-end-capped copolymers of ε-caprolactone and trimethylene carbonate: preparation, photocuring characteristics and surface layering. Biomacromolecules 2002;3:668–75.

[16] Matsuda T, Mizutani M. Liquid acrylate-end-capped biodegradable poly (ε-caprolactone-co-trimethylene carbonate). I. Preparation and visible light-induced photocuring characteristics. J Biomed Mater Res 2002;62:387–94.
[17] Mizutani M, Matsuda T. Liquid acrylate-end-capped biodegradable poly (ε-caprolactone-co-trimethylene carbonate). II. Computer-aided stereolithographic microarchitectural surface photoconstructs. J Biomed Mater Res 2002;62:395–403.
[18] Matsuda T, Kwon IK, Kidoaki S. Photocurable biodegradable liquid copolymers: synthesis of acrylate-end-capped trimethylene carbonate-based prepolymers, photocuring and hydrolysis. Biomacromolecules 2004;5:295–305.